Civil Engineering Infrastructures Journal xx,xx
DOI: 10.22059/CEIJ.2023.361667.1935

Dynamic analysis of thermal crack propagation in roller-compacted concrete dams considering rotational component of ground motion

Tavakoli, H.R. [1*], Mofid, T. [2] and Dehestani, M.[3]

[1]Associate Professor, Faculty of Civil Engineering, Babol Noshirvani University of Technology, Babol, Iran

E-mail: *Tavakoli@nit.ac.ir*

[2] Assistant Professor, Department of Civil Engineering, Urmia University of Technology, Urmia, Iran

E-mail: *T.mofid@chmail.ir*

[3]Professor, Faculty of Civil Engineering, Babol Noshirvani University of Technology, Babol, Iran

E-mail: *Dehestani@nit.ac.ir*

Received: 02/07/2023
Revised: 08/09/2023
Accepted: 25/09/2023

Abstract

In the construction of RCD (Roller-compacted Concrete) dams, two types of internal and external concrete are used; Thermal cracks are occurred due to hydration of various cements in this type of dams. Ignorance of this issue can lead to crack formation in the susceptible points of the dams. In this research, the behavior of the thermal cracks existed in the RCD dam body, is investigated through translational and rotational components of the earthquake. Three-dimensional finite element (FE) model of the concrete dam is built in ABAQUS software, and the model was subjected to 7 earthquake records. After validation of the model, the propagation of the crack existed in the dam body is evaluated using fracture mechanics criterion. The results of the finite element analysis show that the existence of the cracks in the susceptible points of the dam, leads to propagation of these cracks during an earthquake. Especially, with considering the rotational component of the earthquake which has the significant contribution in the obtained values of the crack propagation criterion; This contribution is related to the frequency content of the earthquake, which can lead to an increase of the crack propagation energy up to 50 percent in some earthquake records.

Keywords: Thermal crack propagation, Finite element method, Concrete dam, fracture mechanics criterion

* Corresponding author. Tel.: +98 (0) 111 3231707; fax: +98 (0) 111 3231707
E-mail address: tavakoli@nit.ac.ir

1. Introduction

Crack propagation is one of the most important reasons of concrete dam failures during an earthquake. The first study on the seismic behavior of the concrete gravity dams were performed in 1972 (Chopra & Chakrabarti, 1972). In their study, tensile damages on the dam were shown using linear elastic analysis. In 1989, it was shown that the behavior of the dam was nonlinear under intense earthquakes (El-Aidi & Hall, 1989). In several other studies in 1990, it was demonstrated that the majority of the concrete gravity dams experience cracking even under moderate earthquakes (Ingraffea, 1990; Rescher, 1990). Although many studies have been conducted on the behavior of cracked concrete elements and dams against earthquakes (Alfatlawi et al., 2021; Mofid & Tavakoli, 2020; Mofid & Tavakoli, 2023; Pirooznia & Moradloo, 2020; Priya et al., 2022; Sadeghi & Moradloo, 2022; Singh & Sangle, 2022; Soysal & Arici, 2023; Wang et al., 2022), but fewer studies have been conducted on the behavior of RCD dams against thermal cracks (Hashempour et al., 2023; Koga et al., 2018; Zhang et al., 2020; Zhang et al., 2022). Whereas, RCD dams is widely used as a new method in the dam construction industry. As illustrated in Fig. 1, in the construction of RCD dams, two types of internal and external concrete are used. In the external part of the dam, that is, external concrete, conventional concrete with low permeability is used; In the internal part, roller-compacted concrete with low slump is used; Considering that the nature of internal and external concrete and the cement used in them are different; Therefore, the hydration of different cements in the dam body causes thermal cracks in the external concrete. Neglecting this issue can lead to cracks in vulnerable parts of dams. (Koga et al., 2018). In past researches, limited studies have been done on the effect of earthquake components on the behavior of dams. However, the behavior of thermal cracks created in RCD dams with fracture mechanics criteria has not been done accurately. In this research, the behavior of the thermal cracks existed in the RCD dam body, is investigated through translational and rotational components of the seismic ground motion.

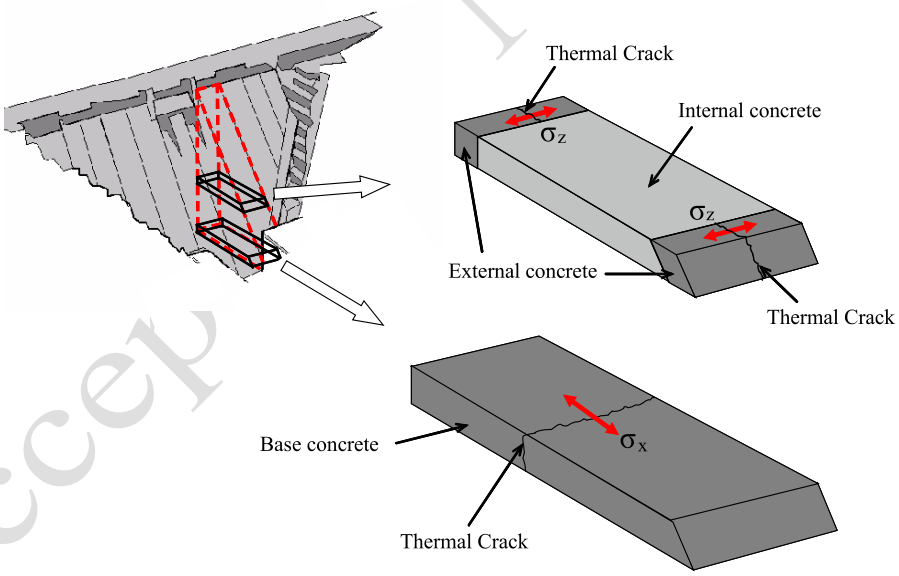

Fig. 1. Position of the thermal cracks in the RCD dam body (Sato et al., 2015)

On the other hand, in most studies on the crack propagation in the concrete dams, only translational component of the earthquake is considered, whereas when an earthquake occurs, rotational components of ground motion are generated which have great effect in the structural responses (Carpiuc-Prisacari et al., 2017; Moradloo & Naiji, 2020). Generally, in earthquake engineering, rotational effect of the earthquake is recognized for the long structures such as bridges, dams, pipe lines, and transfer systems. In earlier studies, the effects of the rotational component were just considered for asymmetric structures (De la Llera & Chopra, 1994; Lee & Trifunac, 1985), whereas some studies demonstrate that there are many symmetric structures which are excited by rotational modes about vertical axis (Takamori et al., 2009;

Teisseyre, 2011). In this paper, the effect of rotational components of earthquake on the behavior of RCD dams is considered.

2. RCD dams introduction

RCD dams are the dams whose concrete is compacted using roller. Because of technical and economic advantages such as reduction in cost and time of construction, this type of dam is widely used by many dam constructors in the world. According to the Fig. 2.a concrete placement of RCD dams is performed by extended layer construction method (ELCM). In ELCM method, the internal concrete of the dam is compacted step by step using rollers. Generally, 15 meters of concrete with a thickness of 1 meter is compacted in each step (Nagataki et al., 2008). As it is clear in Fig. 2.b, the concrete used in RCD dams are divided into two zones of external concrete and internal concrete. The depth of external concrete at upstream and downstream surfaces is 3 m. External concrete is made of conventional concrete while internal concrete is made by RCD method. Slump value of internal concrete must be close to zero to resist the weight of the compaction roller and external conventional concrete must prevent water penetration into the dam body. Due to the difference in the workability of internal and external concrete, the types of these concretes are different. This difference can cause thermal strains and shrinkage between internal and external concretes (Sato et al., 2015). In fact, thermal cracks are generated due to hydration of various cement used in the dam body.

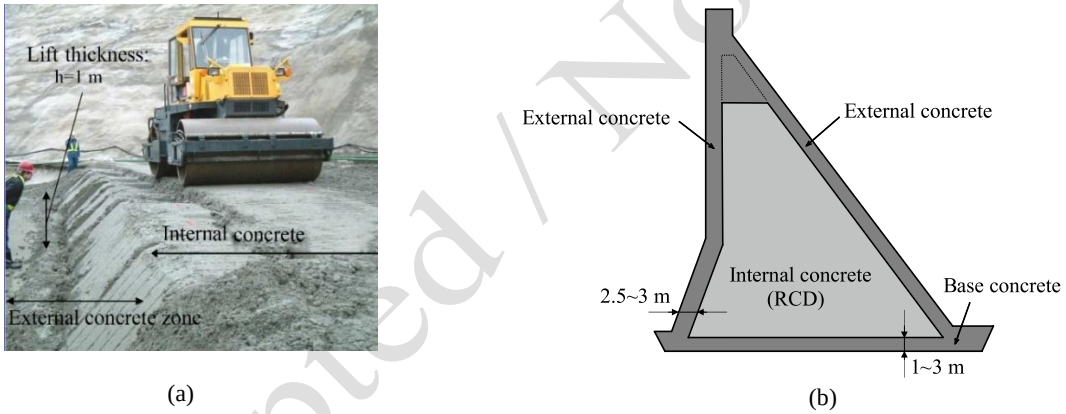

(a) (b)

Fig. 2. Details of RCD dam construction (Nagataki et al., 2008); (a) Internal concrete placement; (b) Internal and external concretes in the RCD dam body.

3. Estimating rotational component of ground motion

In this study, with the aim of more comprehensive investigating the dynamic behavior of the dam, the rotational component of the earthquake is also considered. For this purpose, it is necessary to first calculate the rotational component of the earthquake with methods based on wave theory, which will be briefly explained below. Igel et al. have completely recorded rotational ground motion, using ring laser gyroscope (Igel et al., 2007; Igel et al., 2005). There are different methods proposed by the researchers to estimate the rotational components of the earthquake using two recorded translational components. The first method to estimate rotational component was proposed by Newmark in 1969 (Newmark, 1969). In Newmark method, a simplified relation between translational and rotational components of earthquake was presented, which was investigated more in the further studies. In addition to Newmark method, other methods like time derivative and finite difference methods were also proposed (Ghafory-Ashtiany & Singh, 1986; Li et al., 2004). In this paper, Hong-Nan Li method (Li et al., 2004) is applied to estimate rotational component of the earthquake. Earthquake rotational components are consisted of two rocking components (about x and y axis) and one torsional component (about z axis). In this paper, the rotational component (about y axis) is estimated using horizontal

and vertical components of ground motion (x and z directions). The Hang-Nan Li method (Li et al., 2004) is used for this purpose as follows. Seismic motions are generated by planar harmonic waves and according to Fig. 3 direction of propagation of these waves line in the vertical plane (x, z). These waves are decomposed into in-plane components of amplitude A_S in the plane perpendicular to propagation direction of the waves. The incidence and in-plane of the waves generate two rocking components of ϕ_{gx} and ϕ_{gy} at the free surface (Datta, 2010).

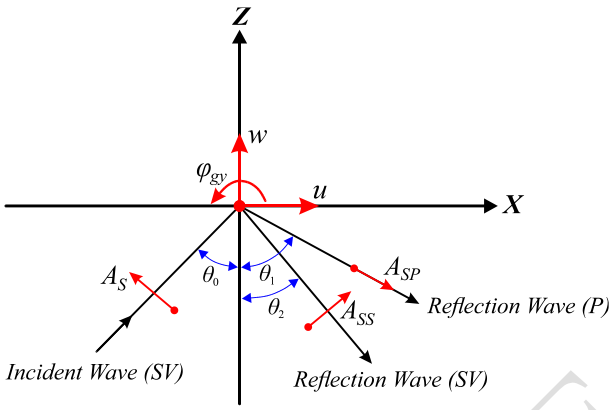

Fig. 3. Propagation of SV wave and its reflection waves on the ground surface (Datta, 2010)

According to Fig. 3, *w* and *u* vectors show positive direction of the ground motion coordinates. *As* and *Ass* vectors show positive direction of the incident waves displacement amplitude and displacement amplitude of *P* and *SV* reflection waves, respectively. θ_0 is the angle of incidence of *SV* waves, θ_1 is the reflection angle of *P* waves and θ_2 is the reflection angle of *SV* waves where θ_0 and θ_2 are equal. In the case of the incident *SV* waves, *u*, *w* and ϕ_{gy} are none-zero components of the motion in y=0 plane. Similarly, for x=0 plane, none-zero components of the motion are *v*, *w* and ϕ_{gx}.

In this study, rotational components of earthquake records are extracted using relations 1 to 16. Based on theory of wave propagation, rocking component (ground motion rotational component about y axis) is equal to:

$$\varphi_{gy} = \frac{1}{2}\left(\frac{\partial w}{\partial x} - \frac{\partial u}{\partial z}\right) \tag{1}$$

Where displacement vectors *u* and *w* in the direction of *x* and *z* are computed as follows:

$$u = \frac{\partial \phi_{SP}}{\partial x} + \frac{\partial(\psi_{SV} + \psi_{SS})}{\partial z} \tag{2}$$

$$w = \frac{\partial \phi_{SP}}{\partial z} - \frac{\partial(\psi_{SV} + \psi_{SS})}{\partial x} \tag{3}$$

For harmonic waves of frequency ω, Potential functions are:

$$\psi_{SV} = A_S \exp i\omega\left(\frac{\sin\theta_0}{\beta}x - \frac{\cos\theta_0}{\beta}z - t\right) \tag{4}$$

$$\varphi_{SP} = A_{SP} \exp i\omega\left(\frac{\sin\theta_1}{\alpha}x + \frac{\cos\theta_1}{\alpha}z - t\right) \tag{5}$$

$$\psi_{SS} = A_{SS} \exp i\omega\left(\frac{\sin\theta_0}{\beta}x + \frac{\cos\theta_0}{\beta}z - t\right) \tag{6}$$

α and β are propagation velocities of *P* and *S* waves, respectively; and can be obtained as follows:

$$\alpha = \left[\frac{E}{\rho}\frac{1-\nu}{(1+\nu)(1-2\nu)}\right]^{\frac{1}{2}} \tag{7}$$

$$\beta = \left[\frac{G}{\rho}\right]^{\frac{1}{2}} = \left[\frac{E}{\rho}\frac{1}{(1+\nu)^2}\right]^{\frac{1}{2}} \tag{8}$$

Where *E*, *G*, ρ, ν are young's modulus, shear modulus, density and Poisson's ratio of soil, respectively. α and β coefficients are dependent to soil condition and are about 5-7 km/sec and 3-4 km/sec for the ground surface, respectively.

By imposing initial condition of free shear stress at the ground surface, we have:

$$\tau_{xz}\Big|_{z=0} = \left[\frac{\partial w}{\partial x} + \frac{\partial u}{\partial z}\right]_{z=0} = 0 \tag{9}$$

Therefore, equation (1) can be rewritten as:

$$\varphi_{gy} = \frac{\partial w}{\partial x} = \frac{\partial^2 \phi_{SP}}{\partial z \partial x} - \frac{\partial^2(\psi_{SV} + \psi_{SS})}{\partial^2 x} = i\omega\frac{\cos\theta_1}{\alpha} i\omega\frac{\sin\theta_1}{\alpha}\phi_{SP} - [(i\omega\frac{\sin\theta_0}{\beta})\psi_{SV} + (i\omega\frac{\sin\theta_0}{\beta})^2\psi_{SS}] \tag{10}$$

According to Snell's law, $\frac{(\sin\theta_0)}{\beta} = \frac{(\sin\theta_1)}{\alpha}$ Therefore we have:

$$\phi_{gy} = \frac{i\omega}{C_x} w \tag{11}$$

Where C_x is equal to $C_x = \beta / \sin\theta_0$. Moreover, The rocking component (ϕ_{gx}) is estimated in the same way. It is clear from equation (11), that, first of all, the angle of incidence must be computed to determine the rocking component. According to the proposed method of Hong Nan Li, with changing the variable $x = \sin\theta_0$ and based on the Snell's law, and also initial condition of free shear stress at the ground surface, the incident angle of SV waves is obtained from equations 12 to 15 as follows (Li et al., 2004):

$$K^2\left(\frac{\partial w}{\partial z} + \frac{\partial u}{\partial x}\right) - 2\frac{\partial u}{\partial x}\Big|_{z=0} = 0 \tag{12}$$

$$\left(\frac{\partial w}{\partial x} + \frac{\partial u}{\partial z}\right)\Big|_{z=0} = 0 \tag{13}$$

$$G = \frac{2x\sqrt{1-K^2x^2}}{K(1-2x^2)}, \qquad \theta_0 < \theta_C \tag{14}$$

$$G = -\frac{2x\sqrt{1-K^2x^2}}{iK(1-2x^2)}, \qquad \theta_0 > \theta_C \tag{15}$$

Where $G = tg\bar{e} = w/u$ and or $G = tg\bar{e} = w/v$ are of the rocking components of the motion in *x-z* and *y-z* planes due to *SV* waves, $K = \alpha/\beta$, $\theta_c = \arcsin(\beta/\alpha)$ incident critical angle and $x = \sin\theta_0$, respectively. To estimate time history of rocking components, equation (11) can be rewritten in the complex form as follows:

$$\varphi_{gy}(t) = \frac{i\omega}{C_x} w = \left(1e^{\frac{\pi}{2}i}\right).\left(\frac{\omega}{C_x}\right).\left(R_w.e^{i\theta_w}\right) = \left(\frac{\omega}{C_x}R_w\right)\left(e^{\left(\frac{\pi}{2}+\theta_w\right)i}\right) \tag{16}$$

Where ω is angular velocity of the wave, *Rw* is the frequency amplitude of the wave in the desired frequency, and θ_w is the phase of the wave in desired frequency, obtained from frequency spectrum of the *w* component. By using discrete Fourier transform and substituting the related equations, the time history of rocking component is obtained (Li et al., 2004). In this paper, 7 near-field earthquake records are used which are given in Table (1).

Table 1 characteristics of the earthquake records

No	Year	Event	Station	Magnitude (Richter)	Closest Distance to Fault Rupture (km)	Shear wave velocity of Soil (m/s)	PGA(g)
1	1999	Kocaeli	Arcelik	7.51	10.56	523.0	0.21
2	1995	Kobe (1)	Takatori	6.90	1.47	256.0	0.61
3	1995	Kobe (2)	Takarazuka	6.90	0.27	312.0	0.69
4	1978	Tabas	Tabas	7.35	2.05	766.7	0.85
5	2003	Bam	Bam	6.60	1.70	487.4	0.79
6	1999	Duzce (1)	Lamont	7.14	9.14	338.0	0.25
7	1999	Duzce(2)	Bolu	7.14	12.02	293.5	0.78

It is obvious that recent earthquakes can also be used, but considering that the vertical component of the earthquakes presented in Table (1) is significant; And on the other hand, many researchers have used these records; Therefore, these 7 earthquakes have been used in this research. Rotational components of these records are extracted using the aforementioned relations (Hong Nan Li relations) and MATLAB software.

4. J integral as a criterion for crack propagation

J integral is considered as one of the fracture mechanics criteria in linear and nonlinear materials and is widely accepted among researchers. This parameter is related to the amount of released energy associated with crack propagation and is regarded as a measure of crack propagation intensity, (especially for nonlinear materials). In this paper, the methods proposed by Parks (1977) and Shih et al. (1986) are used to compute J integral values (Parks, 1977; Shih et al., 1986). The method is considered as one of the appropriate methods because of its simplicity and high accuracy.

This integral is estimated using FE method by ABAQUS software (ABAQUS-Documantation, v2021) and considering equations (17-24). In two dimensional problems, J integral is estimated as follows:

$$\mathrm{J} = \lim_{\Gamma\to 0}\int_{\Gamma} \mathrm{n.H.q}d\Gamma \tag{17}$$

Where Γ defines the minimum path initiating from the bottom crack surface and ending on the top surface (as shown in Fig. 4).

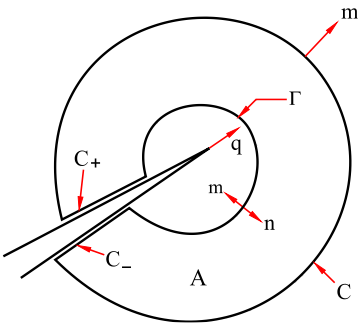

Fig. 4. Two dimensional concept of J integral (ABAQUS-Documantation, v2021)

$\Gamma = 0$ defines the position of the crack tip. *q* defines a unit vector which shows the crack propagation direction and *n* is the outward normal to Γ.

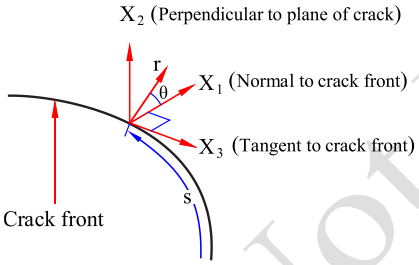

Fig. 5. Three dimensional Concept of J integral (ABAQUS-Documantation, v2021)

According to Fig. 5, J integral value of the three dimensional model is given by:

$$J(s) = \lim_{\Gamma \to 0} \int_{\Gamma} n.H.q d\Gamma \tag{18}$$

For a virtual crack, the released energy rate is defined as follows:

$$\bar{J} = \int_{L} J(s)\lambda(s)ds = \lim_{\Gamma \to 0} \int_{A_t} \lambda(s) n.H.q dA \tag{19}$$

Where L denotes the crack front, dA defines an enclosed area around crack front line, and n is the outward normal to dA. $(dA = ds.d\Gamma)$. Integral of the equation (19) is converted from surface integral into volume integral. According to Fig. 6, an enclosed volume will be generated to compute this integral of three dimensions where *V* denotes the crack front line and the area *A* is consisted of the following terms:

$$A = A_t + A_o + A_{ends} + A_{cracks} \tag{20}$$

Where A_t is the inner enclosed surface around the crack front line, A_o is the outer enclosed surface around the crack front line, A_{cracks} is the crack surface, and A_{ends} is the beginning and ending surface of a closed volume.

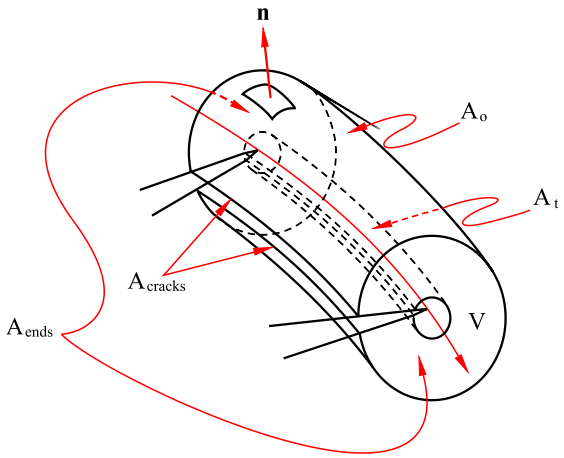

Fig. 6. Enclosed volume to solve the integral

$\bar{q}$ is a weighting function and is defined in a way to have a magnitude of zero on A_o and $\bar{q} = \lambda(s)q$ on A_t. Equation (19) can be rewritten as follows:

$$\bar{J} = -\int_A m.H.\bar{q}dA - \int_{A_{cracks}+A_{ends}} t.\frac{\partial u}{\partial x}.\bar{q}dA \tag{21}$$

Where m is the outward normal to A $(m = -n)$ and t is a surface traction on the surfaces A_{cracks} and A_{ends} $(t = m.\sigma)$. The above equation can be rewritten using divergence theorem as follows:

$$\bar{J} = -\int_V \left[H : \frac{\partial \bar{q}}{\partial x} + (f.\frac{\partial u}{\partial x} - \sigma : \partial \frac{\partial \varepsilon^{th}}{\partial x}).\bar{q} \right] dV - \int_{A_{cracks}+A_{ends}} t.\frac{\partial u}{\partial x}.\bar{q}dA \tag{22}$$

In FE method, to obtain J(s) for the node set P along the crack front line, it is required to consider $\lambda(s)$ as follows:

$$J(s) = N^Q(s)\lambda^Q \tag{23}$$

Where we have $\lambda^Q = 1$ at the node set P and $\lambda^Q = 0$ for the other ones. Equation (23) is substituted in equation (22) and finally equation (22) will be rewritten as follows:

$$J^P = \bar{J}^P / \int_L N^P ds \tag{24}$$

J integral value is equal to the released strain energy of G, Therefore, the critical released strain energy can be utilized to use J integral as a crack propagation criterion (Gdoutos, 2012). G_c rate is varied for different kinds of concrete and its maximum value is $166.71(\frac{N}{m})$ (Shah & Kishen, 2011).

5. Finite element modeling of the dam

There are many analytical and experimental studies on the gravity concrete dams and Koyna dam is used as a benchmark dam in many of these studies, because of the statistical data which are recorded after Koyna earthquake and are comparable with the theory based analysis results (Chopra & Chakrabarti, 1973; Kianoush, 2008). Therefore, in this research, Koyna dam is used as a benchmark structure. As it is clear in Fig. 7 it has 103 meters height and 850 meters length, located in India. This dam was subjected to Koyna earthquake of 6.5 Richter scale magnitude and gone thorough serious damages and cracking. The water level behind the dam was 91.75 meters, the hydrostatic pressure of which must be considered. In this study, due to the large length to width ratio of the dam, plain strain relations are used to solve the governing equations; On the other hand, it is obvious that considering the interaction of soil and structure has a significant effect on the behavior of the dam; However, in order to simplify the problem and reduce the time of analysis, in this study, the dam base is assumed to be fixed. As mentioned in section 2, concrete placing of RCD dams is performed by

ELCM method; In this method, the thickness of each layer is equal to 1 meter. The construction of each layer is conducted in several step, in each step, 15 meters of the length of the dam is compacted. Therefore, in this research, a three-dimensional FE model was constructed for a block of dam with 15 m length. In order to consider plain strain relations, the displacement perpendicular to the dam length was constrained (Fig. 7b). Material characteristics and natural frequency of Koyna dam are given in Tables 2 and 3 respectively. Concrete damaged plasticity is used for introducing the concrete behavior (Lee & Fenves, 1998; Lubliner et al., 1989). In this model, concrete behavior is introduced separately in tension and compression. In addition, uniaxial tension damage parameter of the concrete is applied in accordance with the displacement of the crack.

Table 2 Material properties for the Koyna dam concrete (Chopra & Chakrabarti, 1973)

Parameter	Value
Young's modulus	E = 31027 MPa
Poisson's ratio	$\upsilon = 0.15$
Density	$\rho = 2643$ kg/m^3
Dilation angle	$\psi = 36.31^o$
Compressive initial yield stress	$\sigma_{c0} = 13.0$ MPa
Compressive ultimate stress	$\sigma_{cu} = 24.1$ MPa
Tensile failure stress	$\sigma_{t0} = 2.9$ MPa

Table 3 Natural frequencies of the Koyna dam (Chopra & Chakrabarti, 1973)

Mode	Natural Frequency (rad sec^{-1})	
	Abaqus	Chopra and Chakrabarti (1973)
1	18.86	19.27
2	49.97	51.50
3	68.16	67.56
4	98.27	99.73

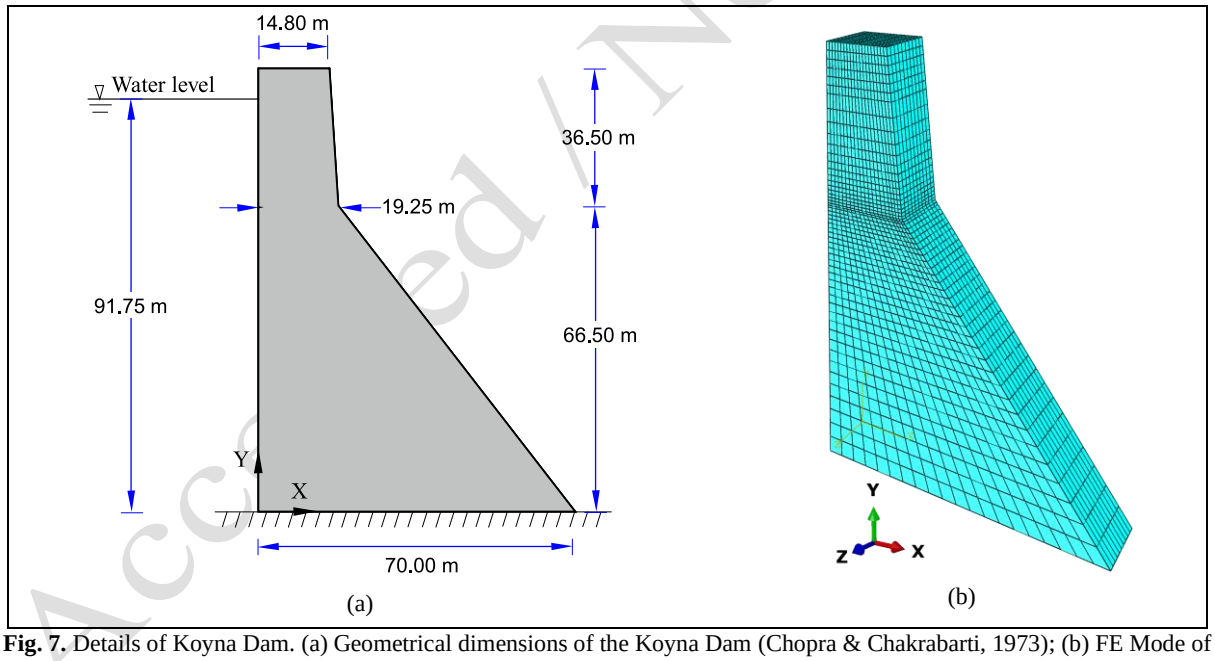

Fig. 7. Details of Koyna Dam. (a) Geometrical dimensions of the Koyna Dam (Chopra & Chakrabarti, 1973); (b) FE Mode of Koyna Dam

Damping coefficient of the conventional dams is 2-3 percent which is considered 3 percent in this research. To introduce damping, it is first required to compute β coefficient as follows:

$$\beta = \frac{2\xi_1}{\omega_1} \tag{25}$$

Where ξ_1 is the critical damping of the first mode and ω_1 is the natural frequency of the first mode, which are given in Table (3). Natural frequency of the first mode is 18.86, Therefore, β is obtained 3.23 10^{-3} sec.

6. Validation of the finite element model

The model was subjected to the accelerograms of Koyna earthquake, as provided in Fig. 8 and finite element results are compared with shake table experimental results (Wilcoski et al., 2001) and the reference model results (Kianoush, 2008). Owing to the fact that tensile strength of the concrete is much lower than compressive strength; the concrete will fail in tension. As it is clear in Fig. 9 the cracking is initiated from the interface of the structure and foundation from the upstream region (dam heel) and grows to some extent and then stops. Then, the cracking in the upper one-third region of the dam is initiated from the downstream (dam throats) which then propagates to the upstream region of the dam.

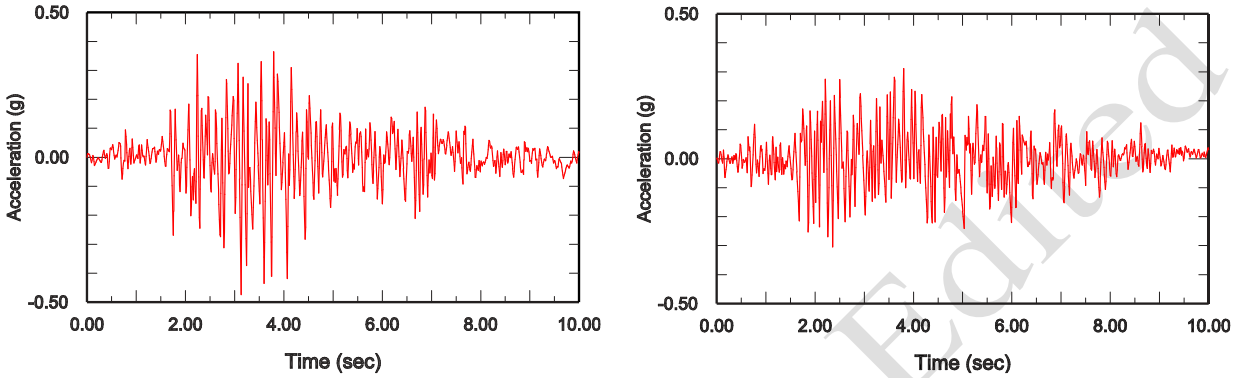

Fig. 8. Koyna earthquake accelerograms (a) horizontal acceleration; (b) vertical acceleration

As it is shown in Fig. 10 in the FE model, shaking table model (Wilcoski et al., 2001) and the reference model (Kianoush, 2008), the position of the crack growth is the same. Fig. 11 also compares the relative displacement of the dam crest, with the results of the reference model and shows a little difference between them. Also, comparing the results of FE model analysis with several other numerical models (Haghani et al., 2020; Haghani et al., 2021, 2022) shows that the constructed model has good accuracy. Therefore, it can be concluded that the FE model built in this research, is valid.

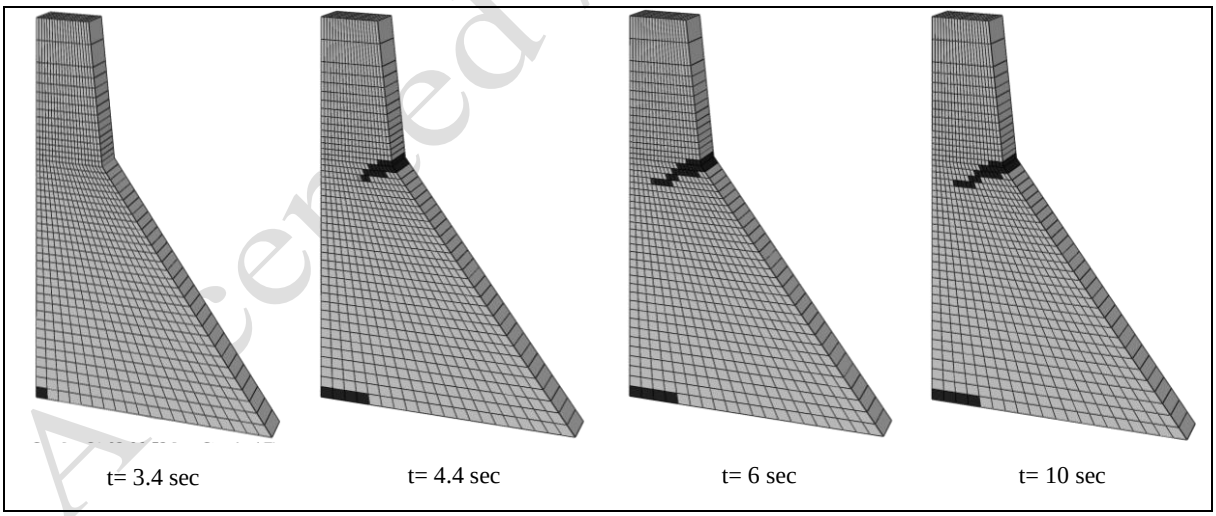

Fig. 9. Crack growth after imposing Koyna earthquake

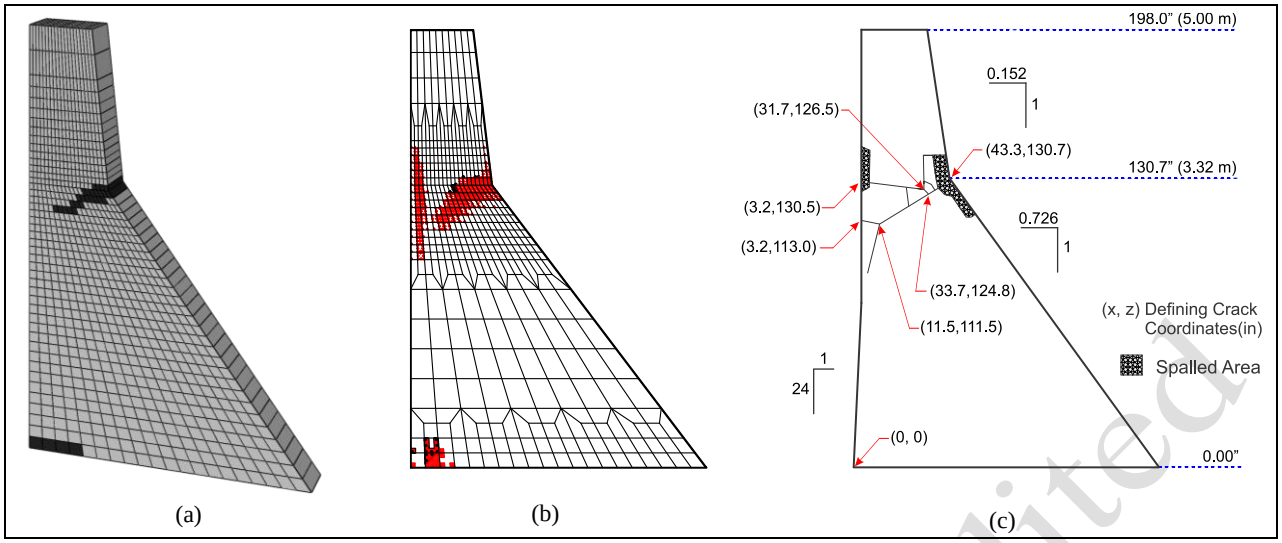

Fig. 10. FE model validation (a) tensile failure of the concrete after finite element analysis; (b) reference model results (Kianoush, 2008) (c) Results obtained from the shaking table (Wilcoski et al., 2001).

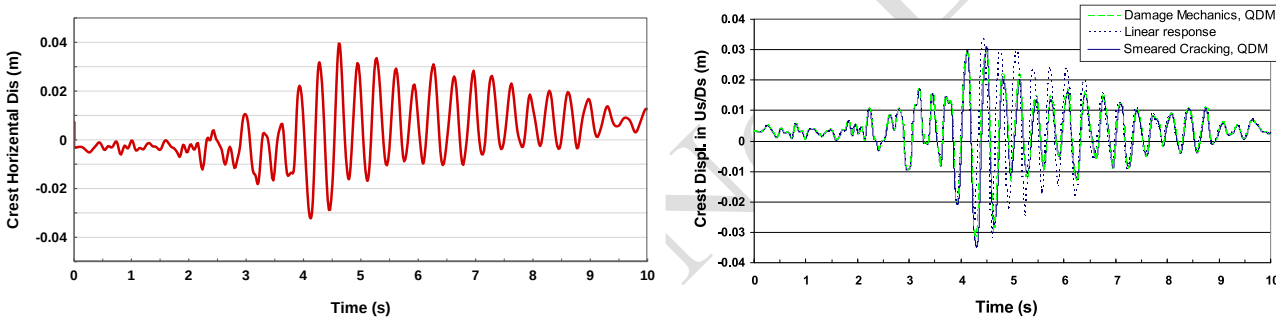

Fig. 11. FE model validation (a) relative displacement of the dam crest in the FE model; (b) reference model results (Kianoush, 2008)

7. Thermal crack modeling

Results of the FE model show that the critical regions of the dam during an earthquake are the upper one-third region of the dam from the downstream side (dam throat) and the interface of the structure and foundation form the upstream side (dam heel), where the dam throat is the most critical region of the dam from seismic point of view. In this paper, as shown in Fig. 12 the behavior of a thermal crack is evaluated supposing the crack is located at the dam throat, where is the most critical region on the dam. The crack length is equal to the external concrete thickness (3 m) and the crack height is equal to the thickness of the RCD concrete (1 m). According to the mentioned details, this crack is generated at the height of 66.5 m in the FE model and is evaluated under 7 earthquake records which were introduced in the Table (1).

8. Finite element analysis results

The FE model is subjected to the rotational and translational components of the earthquake records mentioned in Table (1) and the results of the nonlinear FE analysis are then evaluated. To validate J integral method, the crack behavior is evaluated using concrete tensile damage method under one of the earthquake records and the results are compared with the estimated values of J integral. Then, the crack behavior is also evaluated under 6 remaining earthquake records. Fig. 13 shows the results of the FE analysis on Koyna dam under Kocaeli earthquake (1999) for two conditions of regarding rotational component and neglecting it. The FE analysis results of this dam under Kocaeli earthquake are summarized

in Table (4). In this table, the obtained values refer to the maximum relative displacement of the dam, maximum base shear, and maximum J integral value, for both conditions. It can be seen that taking into account of the rotational component leads to 2 percent reduction in the maximum displacement response and 20 percent reduction in maximum base shear response of the dam; while the J integral estimated value of the three components condition is about twice of the two component condition value.

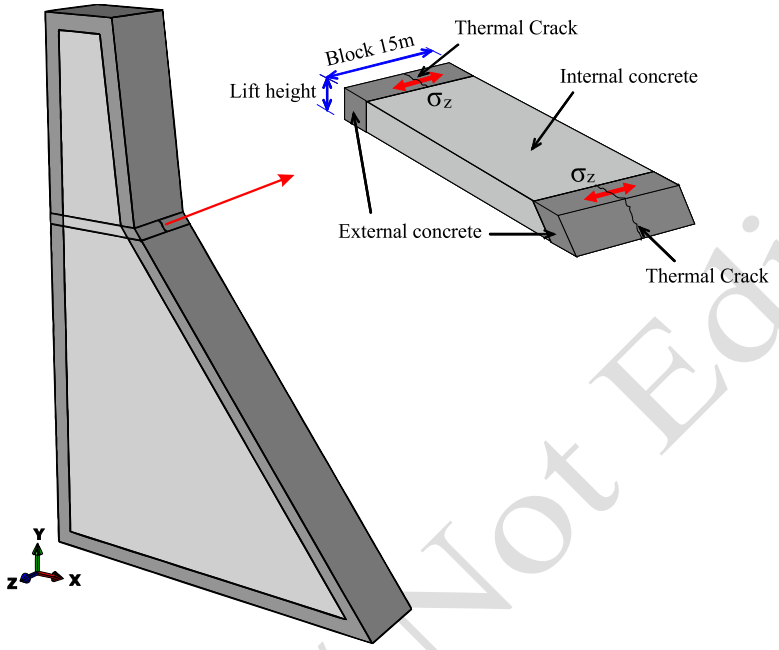

Fig. 12. Thermal crack location in the finite element model

It can be seen in Fig. 13 that in two components condition, concrete tensile damage is not present at the crack location, which means the crack is not propagated, while in three components condition, the first tensile damage is formed and the crack is ready to propagate. By comparing maximum values of J integral mentioned in table (4), and the values provided by reference (Shah & Kishen, 2011), it can be concluded that in two components condition, the J integral estimated value is lower than the critical released strain energy G_C=166.71 (N/m) While it is higher in three components condition. Therefore, it can be concluded that J integral is an appropriate criterion to evaluate crack propagation in this model and has enough accuracy. The tensile damage related to the remaining earthquake records mentioned in Table 1 is shown in Fig. 14 for both conditions.

Table 4 The results obtained from the finite element analysis under Kocaeli earthquake (1999)

Parameter	Maximum displacement of the dam crest (mm)	Maximum base shear of the dam (N)	Maximum J integral value (N/m)
2 Components condition (neglecting rotational component)	20.23	324.2×10^6	106.49
3 Components condition (considering rotational component)	19.98	259.5×10^6	202.50
The ratio of 3 Component to 2 Component	0.98	0.80	1.90

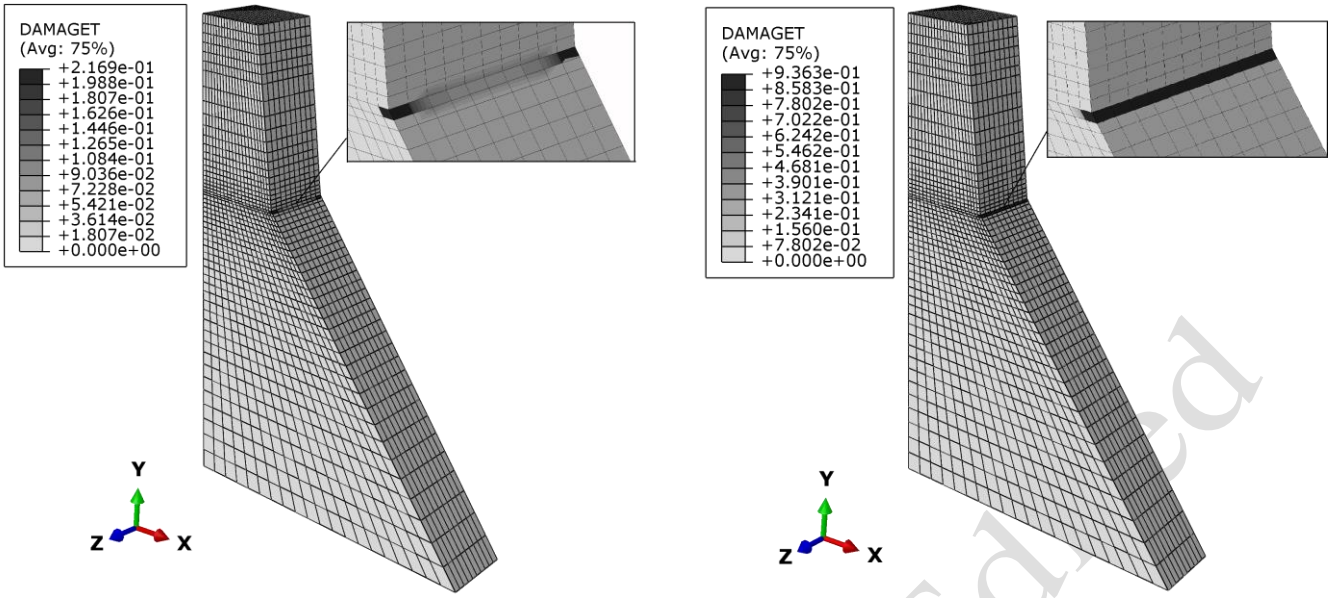

Fig. 13. Concrete tensile damage under Kocaeli earthquake (1999); (a) neglecting rotational component (2 Components condition); (b) considering rotational component (3 Components condition).

The obtained values of the maximum relative displacement of the dam crest, maximum base shear, and maximum J integral value, for both conditions are summarized in Table 5. Comparing response ratios of two components and three components conditions, it can be concluded that considering rotational component can change relative displacement of the dam crest and maximum base shear of the dam up to 25 percent and this change can be either increasing or decreasing in respect to intensity and frequency content of the earthquake. The results of imposing seven records show that considering rotational components often has decreasing effect in terms of maximum displacement of the dam crest, while this consideration has increasing effect in terms of maximum base shear of the dam. Rotational components also have considerable effect on J integral estimated values, for instance, earthquake records of Kacaeli (1999) and Kobe 2 (1995), cause more than 50 percent increase in J integral values. As it was mentioned before, the released strain energy in the thermal crack tip, is equal the estimated J integral value in table (5), where the maximum value of this integral is for Tabas earthquake (1978) 126.7×10^{3} (N/m) and the minimum value was for Duzce1 earthquake (1999) 32.95 (N/m). Therefore, it is expected that the maximum and minimum failure due to thermal crack propagation are related to these earthquake records, Fig. 14 confirms this issue.

Table 5 summarized results obtained from finite element analysis for different earthquake records

Event	Maximum displacement of the dam crest (mm)			Maximum base shear of the dam (N) $\times10^{6}$			Maximum J integral value (N/m)		
	2Comp*	**3Comp***	**R****	**2Comp***	**3Comp***	**R****	**2Comp***	**3Comp***	**R****
Kocaeli(1999)	20.2	19.9	0.98	324.2	259.5	0.80	106.49	202.5	1.90
Kobe 1 (1995)	286.9	282.1	0.98	815.6	786.2	0.96	48.36×10^{3}	36.1×10^{3}	0.75
Kobe 2 (1995)	64.7	59.4	0.92	934.4	933.7	0.99	6.74×10^{3}	10.2×10^{3}	1.51
Tabas (1978)	115.6	120.0	1.04	1093.2	1336.4	1.22	262.5×10^{3}	126.7×10^{3}	0.48
Bam (2003)	117.9	115.9	0.98	815.6	923.4	1.13	37.92×10^{3}	41.0×10^{3}	1.08
Duzce1(1999)	20.5	23.4	1.14	893.1	924.7	1.03	18.71	32.9	1.76
Duzce2(1999)	168.8	167.2	0.99	837.2	1058.5	1.26	14.48×10^{3}	13.5×10^{3}	0.93

2Comp*: 2 Components condition (Neglecting rotational component)
3Comp*: 3 Components condition (Considering rotational component)
R** : The ratio of 3Comp to 2Comp

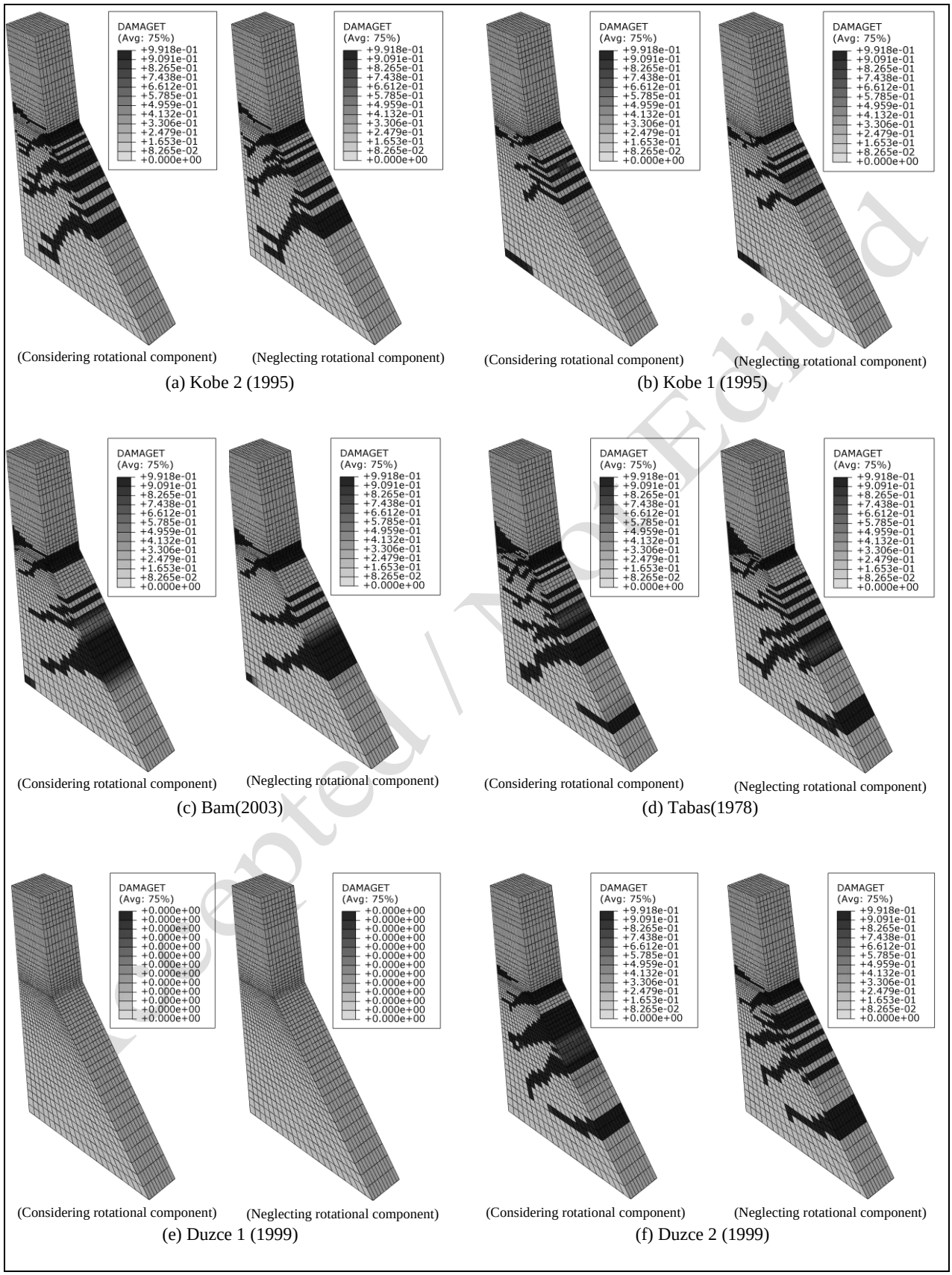

Fig. 14. Concrete tensile damage under earthquake rotational and translational components

9. Conclusion

In this study, the behavior of thermal cracks existed in the concrete dam body, is evaluated under rotational and translational components of the earthquakes. First, three dimensional model of Koyna dam was built in ABAQUS software using finite element method and subjected to 7 near field earthquake records. Comparing the results of FE model with experimental data revealed that the built finite element model is valid. Then, a thermal crack with 3 m length at the height of 66.5 m from the dam bottom was modeled in downstream side of the dam and the released strain energy due to the crack propagation was obtained using J integral as a fracture criterion, under rotational and translational components of 7 earthquake records.

The obtained results from finite element analysis are represented as follows:

- Comparing the obtained results from the concrete tensile damage with J integral estimated values, it can be concluded that J integral is an appropriate fracture criterion to evaluate crack propagation in concrete dams and has enough accuracy.
- Considering the rotational components of an earthquake, can change seismic response of the dam up to 25 percent and this change can be either in form of decreasing or increasing in respect to intensity and frequency content of the earthquake.
- Rotational components of the earthquake records often have decreasing effect in the maximum displacement of the dam crest whereas for base shear, rotational components have increasing effect.
- In comparison with other seismic parameters, rotational components of the earthquake have more significant effect on J integral values, for instance, earthquake records of Kocaeli (1999) and Kobe 2 (1995) show 50 percent increase in J integral values.

10. Acknowledgments

This research was funded by the Babol Noshirvani University of Technology under Grant No. BUT/388011/1401.

11. References

ABAQUS-Documantation. (v2021). *Abaqus Theory Guide*. J-integral evaluation.

Alfatlawi, T. J. M., Kadhim, M. J., & Hussein, M. N. (2021). Relation between cracks behavior and curvature in cracked concrete arch dam under earthquake. *Materials Today: Proceedings*. https://doi.org/https://doi.org/10.1016/j.matpr.2021.02.248

Carpiuc-Prisacari, A., Poncelet, M., Kazymyrenko, K., Leclerc, H., & Hild, F. (2017). A complex mixed-mode crack propagation test performed with a 6-axis testing machine and full-field measurements. *Engineering Fracture Mechanics*, *176*, 1-22. https://doi.org/https://doi.org/10.1016/j.engfracmech.2017.01.013

Chopra, A. K., & Chakrabarti, P. (1972). The earthquake experience at Koyna dam and stresses in concrete gravity dams. *Earthquake Engineering & Structural Dynamics*, *1*(2), 151-164. https://doi.org/https://doi.org/10.1002/eqe.4290010204

Chopra, A. K., & Chakrabarti, P. (1973). The Koyna earthquake and the damage to Koyna dam. *Bulletin of the Seismological Society of America*, *63*(2), 381-397.

Datta, T. K. (2010). *Seismic analysis of structures*. John Wiley & Sons.

De la Llera, J. C., & Chopra, A. K. (1994). Accidental torsion in buildings due to stiffness uncertainty. *Earthquake Engineering & Structural Dynamics*, *23*(2), 117-136. https://doi.org/https://doi.org/10.1002/eqe.4290230202

El-Aidi, B., & Hall, J. F. (1989). Non-linear earthquake response of concrete gravity dams part 1: modelling. *Earthquake Engineering & Structural Dynamics*, *18*(6), 837-851. https://doi.org/https://doi.org/10.1002/eqe.4290180607
Gdoutos, E. E. (2012). *Fracture mechanics criteria and applications* (Vol. 10). Springer Science & Business Media.
Ghafory-Ashtiany, M., & Singh, M. P. (1986). Structural response for six correlated earthquake components. *Earthquake Engineering & Structural Dynamics*, *14*(1), 103-119. https://doi.org/https://doi.org/10.1002/eqe.4290140108
Haghani, M., Navayi Neya, B., & Ahmadi, M. T. (2020). Nonlinear Seismic Analysis of Concrete Gravity Dams Using Extended Finite Element method and Plastic Damage Model. *Modares Civil Engineering journal*, *20*(3), 189-201.
Haghani, M., Neya, B. N., Ahmadi, M. T., & Amiri, J. V. (2021). Comparative Study of Smeared Crack and Extended Finite Element Method for Predicting the Crack Propagation in Concrete Gravity Dams. *Journal of Earthquake Engineering*, 1-34. https://doi.org/https://doi.org/10.1080/13632469.2021.1991513
Haghani, M., Neya, B. N., Ahmadi, M. T., & Amiri, J. V. (2022). A new numerical approach in the seismic failure analysis of concrete gravity dams using extended finite element method. *Engineering Failure Analysis*, *132*, 105835. https://doi.org/https://doi.org/10.1016/j.engfailanal.2021.105835
Hashempour, S. A., Akbari, R., & Lotfi, V. (2023). A simplified continuum damage model for nonlinear seismic analysis of concrete arch dams using different damping algorithms. *Civil Engineering Infrastructures Journal*.
Igel, H., Cochard, A., Wassermann, J., Flaws, A., Schreiber, U., Velikoseltsev, A., & Pham Dinh, N. (2007). Broad-band observations of earthquake-induced rotational ground motions. *Geophysical Journal International*, *168*(1), 182-196. https://doi.org/https://doi.org/10.1111/j.1365-246X.2006.03146.x
Igel, H., Schreiber, U., Flaws, A., Schuberth, B., Velikoseltsev, A., & Cochard, A. (2005). Rotational motions induced by the M8. 1 Tokachi-oki earthquake, September 25, 2003. *Geophysical Research Letters*, *32*(8). https://doi.org/https://doi.org/10.1029/2004GL022336
Ingraffea, A. (1990). Case studies of simulation of fracture in concrete dams. *Engineering Fracture Mechanics*, *35*(1-3), 553-564. https://doi.org/https://doi.org/10.1016/0013-7944(90)90230-E
Kianoush, H. M. a. M. (2008). SEISMIC SAFETY EVALUATION OF CONCRETE DAMS USING DAMAGE MECHANICS APPROACH.
Koga, H., Katahira, H., & Kawano, H. (2018). Thermal measurement and analysis of large Roller Compacted Concrete dam. In *Roller Compacted Concrete Dams* (pp. 1139-1147). Routledge.
Lee, J., & Fenves, G. L. (1998). Plastic-damage model for cyclic loading of concrete structures. *Journal of engineering mechanics*, *124*(8), 892-900.
Lee, V. W., & Trifunac, M. D. (1985). Torsional accelerograms. *International Journal of Soil Dynamics and Earthquake Engineering*, *4*(3), 132-139. https://doi.org/https://doi.org/10.1016/0261-7277(85)90007-5
Li, H.-N., Sun, L.-Y., & Wang, S.-Y. (2004). Improved approach for obtaining rotational components of seismic motion. *Nuclear Engineering and Design*, *232*(2), 131-137. https://doi.org/https://doi.org/10.1016/j.nucengdes.2004.05.002
Lubliner, J., Oliver, J., Oller, S., & Onate, E. (1989). A plastic-damage model for concrete. *International Journal of solids and structures*, *25*(3), 299-326.
Mofid, T., & Tavakoli, H. (2020). Experimental investigation of post-earthquake behavior of RC beams. *Journal of Building Engineering*, *32*, 101673. https://doi.org/https://doi.org/10.1016/j.jobe.2020.101673
Mofid, T., & Tavakoli, H. (2023). Experimental investigation of mechanical behavior of lightweight RC elements under repeated loadings. Structures,
Moradloo, A. J., & Naiji, A. (2020). Effects of rotational components of earthquake on seismic response of arch concrete dams. *Earthquake Engineering and Engineering Vibration*, *19*(2), 349-362. https://doi.org/https://doi.org/10.1007/s11803-020-0566-x
Nagataki, S., Fujisawa, T., & Kawasaki, H. (2008). State of art of RCD dams in Japan. 50º Congresso brasileiro do concreto, Salvado (1st Brazilian RCC Symposium september 2008),
Newmark, N. M. (1969). Torsion in symmetrical buildings.
Parks, D. (1977). The virtual crack extension method for nonlinear material behavior. *Computer methods in applied mechanics and engineering*, *12*(3), 353-364.
Pirooznia, A., & Moradloo, A. (2020). Investigation of size effect and smeared crack models in ordinary and dam concrete fracture tests. *Engineering Fracture Mechanics*, *226*, 106863. https://doi.org/https://doi.org/10.1016/j.engfracmech.2019.106863
Priya, M., PriyaPriya, M., & Santhi, A. (2022). A material model approach on the deflection and crack pattern in different panels of the RCC flat plate using finite element analysis. *Civil Engineering Journal*, *8*(3), 472-487.
Rescher, O.-J. (1990). Importance of cracking in concrete dams. *Engineering Fracture Mechanics*, *35*(1-3), 503-524. https://doi.org/https://doi.org/10.1016/0013-7944(90)90226-7
Sadeghi, M. H., & Moradloo, J. (2022). Seismic analysis of damaged concrete gravity dams subjected to mainshock-aftershock sequences. *European Journal of Environmental and Civil Engineering*, *26*(6), 2417-2438. https://doi.org/https://doi.org/10.1080/19648189.2020.1763475

Sato, H., Miyazawa, S., & Yatagai, A. (2015). Thermal crack estimation of dam concrete considering the influence of autogenous shrinkage. In *CONCREEP 10* (pp. 1289-1298). https://doi.org/https://doi.org/10.1061/9780784479346.153

Shah, S., & Kishen, J. C. (2011). Fracture properties of concrete–concrete interfaces using digital image correlation. *Experimental mechanics*, *51*(3), 303-313.

Shih, C., Moran, B., & Nakamura, T. (1986). Energy release rate along a three-dimensional crack front in a thermally stressed body. *International Journal of fracture*, *30*(2), 79-102.

Singh, V., & Sangle, K. (2022). Analysis of vertically oriented coupled shear wall interconnected with coupling beams. *HighTech and Innovation Journal*, *3*(2), 230-242. https://doi.org/https://doi.org/10.28991/HIJ-2022-03-02-010

Soysal, B. F., & Arici, Y. (2023). Crack Width–Seismic Intensity Relationships for Concrete Gravity Dams. *Journal of Earthquake Engineering*, 1-17. https://doi.org/https://doi.org/10.1080/13632469.2023.2220048

Takamori, A., Araya, A., Otake, Y., Ishidoshiro, K., & Ando, M. (2009). Research and development status of a new rotational seismometer based on the flux pinning effect of a superconductor. *Bulletin of the Seismological Society of America*, *99*(2B), 1174-1180. https://doi.org/https://doi.org/10.1785/0120080087

Teisseyre, R. (2011). Why rotation seismology: Confrontation between classic and asymmetric theories. *Bulletin of the Seismological Society of America*, *101*(4), 1683-1691. https://doi.org/https://doi.org/10.1785/0120100078

Wang, Y.-J., Wu, Z.-M., Qu, F.-M., & Zhang, W. (2022). Numerical investigation on crack propagation process of concrete gravity dams under static and dynamic loads with in-crack reservoir pressure. *Theoretical and Applied Fracture Mechanics*, *117*, 103221. https://doi.org/https://doi.org/10.1016/j.tafmec.2021.103221

Wilcoski, J., Hall, R. L., Gambill, J. B., Matheu, E. E., & Chowdhury, M. R. (2001). *Seismic testing of a 1/20 scale model of Koyna dam*.

Zhang, M., Li, M., Zhang, J., Liu, D., Hu, Y., Ren, Q., & Tian, D. (2020). Experimental study on electro-thermal and compaction properties of electrically conductive roller-compacted concrete overwintering layer in high RCC dams. *Construction and Building Materials*, *263*, 120248. https://doi.org/https://doi.org/10.1016/j.conbuildmat.2020.120248

Zhang, X., Yan, T., Liu, Q., Zhang, X., & Wang, L. (2022). Cracking analysis of induced joints in roller compacted concrete arch dam. *Alexandria Engineering Journal*, *61*(5), 3599-3612. https://doi.org/https://doi.org/10.1016/j.aej.2021.08.082